

## First-Principles Investigation of the $\text{TiO}_2$ /Organohalide Perovskites Interface: The Role of Interfacial Chlorine

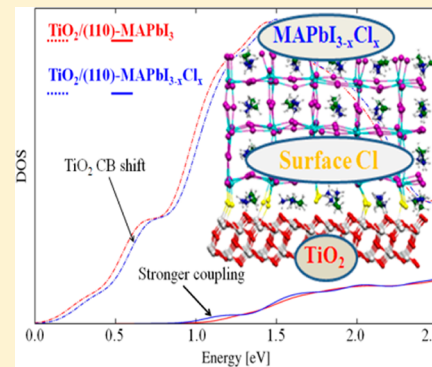
Edoardo Mosconi\*,† Enrico Ronca, †,‡ and Filippo De Angelis\*,†

†Computational Laboratory for Hybrid/Organic Photovoltaics (CLHYO), Istituto CNR di Scienze e Tecnologie Molecolari (CNR-ISTM), Via Elce di Sotto 8, I-06123 Perugia, Italy

‡Department of Chemistry, Biochemistry and Biotechnologies, University of Perugia, Via Elce di Sotto 8, I-06123 Perugia, Italy

### Supporting Information

**ABSTRACT:** We investigate the prototypical interface between organohalide perovskites and  $\text{TiO}_2$  by first-principles electronic structure calculations. The investigated heterointerface is representative of conventional dye-sensitized solar cells based on a mesoporous  $\text{TiO}_2$  scaffold and of flat devices in which a compact  $\text{TiO}_2$  film is used as electron selective layer. We find that the  $\text{MAPbI}_3$  and  $\text{MAPbI}_{3-x}\text{Cl}_x$  perovskites tend to grow in (110)-oriented films on  $\text{TiO}_2$ , due to the better structural matching between rows of adjacent perovskite surface halides and  $\text{TiO}_2$  undercoordinated titanium atoms. Interfacial chlorine atoms further stabilize the (110) surface, due to an enhanced binding energy. We find that the stronger interaction of  $\text{MAPbI}_{3-x}\text{Cl}_x$  with  $\text{TiO}_2$  modifies the interface electronic structure, leading to a stronger interfacial coupling and to a slight  $\text{TiO}_2$  conduction band energy upshift. Our modeling study may constitute the basis for a further exploitation of perovskite solar cells.



### SECTION: Energy Conversion and Storage; Energy and Charge Transport

**H**ybrid lead-halide perovskites are revolutionizing the landscape of emerging photovoltaic technologies. From their first application in 2009 by Kojima et al. as solar cell sensitizers,<sup>1</sup> photovoltaic devices based on these materials showed a fast and continuous increase in their efficiency,<sup>2,3</sup> with very recent certified efficiency close to 18%. Organohalide-lead perovskites can be solution-processed at low temperature<sup>4</sup> and vapor-deposited,<sup>2</sup> realistically holding the promise to reach comparable efficiency as conventional thin-film photovoltaic technologies. Furthermore, these materials can be combined with organic electron acceptors/donors, to deliver flexible photovoltaic devices.<sup>5,6</sup>

Perhaps, the most intriguing feature of hybrid perovskites is that they can support both electron and hole transport.<sup>4,7,8</sup> Thus, if on the one hand these materials can be employed as solar cell sensitizers when deposited on *n*-transporting mesoporous  $\text{TiO}_2$ , in traditional dye-sensitized solar cells, on the other hand, meso-superstructured and planar heterojunction solar cells can be fabricated in which the perovskite serves as light absorber and electron transporter. A depleted perovskite layer deposited on mesoporous  $\text{TiO}_2$  was also shown to transport holes to an Au-cathode directly evaporated on top of the perovskite.<sup>7</sup>

Methylammonium lead-iodide, hereafter  $\text{MAPbI}_3$ , and the related mixed halide  $\text{MAPbI}_{3-x}\text{Cl}_x$  analogue have dominated the field. Meso-superstructured and planar heterojunction solar cells were successfully implemented with  $\text{MAPbI}_{3-x}\text{Cl}_x$ ,<sup>2,8</sup> but the same devices based on the prototype  $\text{MAPbI}_3$  perovskite showed comparably lower performances.<sup>9</sup> This behavior,

initially interpreted on the basis of the improved carrier mobility of  $\text{MAPbI}_{3-x}\text{Cl}_x$  compared to that of  $\text{MAPbI}_3$ ,<sup>9</sup> was later ascribed to a reduced carrier recombination of  $\text{MAPbI}_{3-x}\text{Cl}_x$ .<sup>10</sup> A possibly related phenomenon is the observation of improved charge transport in dye-sensitized solar cells based on  $\text{MAPbI}_{3-x}\text{Cl}_x$  and  $\text{MAPbI}_{3-x}\text{Br}_x$ ,<sup>11,12</sup> leading to enhanced photocurrent or open circuit voltage compared to that of  $\text{MAPbI}_3$ . Similarly, Suarez et al. and Gonzalez-Pedro et al. recently reported improved photovoltaic performances of  $\text{MAPb}(\text{I}_{1-x}\text{Br}_x)_{3-y}\text{Cl}_y$  perovskites in both dye-sensitized and thin film solar cells in relation to a reduced recombination behavior.<sup>13,14</sup>

In spite of the success of  $\text{MAPbI}_{3-x}\text{Cl}_x$  mixed halide perovskite, the intimate materials properties underlying its superior photovoltaic performance and, in particular, the role of chlorine in the material are not clear, beyond the phenomenological observation of reduced carrier recombination or improved transport. Surprisingly, even the material composition is still uncertain, although combined X-ray diffraction data and computational analyses point at only a small Cl-incorporation (~1–4%) into the  $\text{MAPbI}_3$  lattice,<sup>11</sup> in line with the predicted thermodynamically unfavorable formation of solid  $\text{MAPbI}_3/\text{MAPbCl}_3$  solutions.<sup>15,16</sup> Colella et al. indeed reported the same tetragonal structure for  $\text{MAPbI}_3$  and  $\text{MAPbI}_{3-x}\text{Cl}_x$ , with a cell volume contraction of only 0.7% in the latter.<sup>11</sup> Zhao and

Received: June 4, 2014

Accepted: July 9, 2014

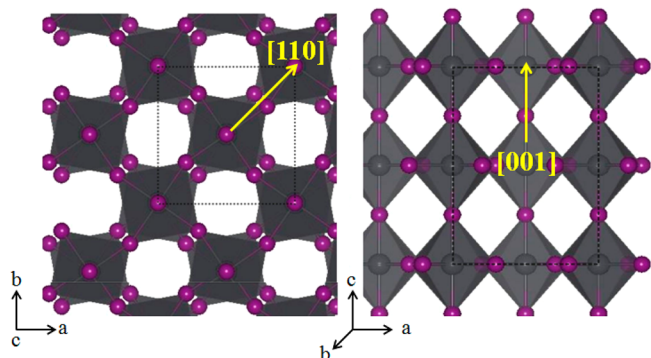
Published: July 9, 2014



Zhu also very recently reported on the beneficial effect on the photovoltaic properties of adding the  $\text{M}\text{A}\text{Cl}$  salt to the standard preparation of  $\text{MAPbI}_3$ , suggesting a role of chlorine in assisting the perovskite growth, though energy dispersive X-ray (EDX) analysis of the annealed perovskite film did not reveal the presence of chlorine within the technique detection limit ( $\sim 1\%$ ).<sup>17</sup> Similarly, Edri et al. reported a significant improvement on the photovoltaic performance of the  $\text{MAPbBr}_{3-x}\text{Cl}_x$  perovskite compared to that of its nonchlorinated analogue.<sup>18</sup> Because no chlorine was detected in the film by EDX but X-ray photoelectron spectroscopy showed a few percent of Cl in the material, these authors concluded that chlorine was possibly concentrated at/near the surface.<sup>18</sup>

Apart from the slight change in absorption spectra<sup>19</sup> and small volume contraction,<sup>11</sup> a characteristic of  $\text{MAPbI}_{3-x}\text{Cl}_x$  perovskites is their tendency to grow oriented along the [110] direction,<sup>2,8,11,20</sup> Scheme 1 and Figure 1, as originally

**Scheme 1.** Schematics of the  $\text{MAPbI}_3$  XRD Structure Viewed along the *c* Axis (Left) and *ab* Plane (Right)<sup>a</sup>



<sup>a</sup>Notice the sizable octahedra tilting typical of the  $\text{MAPbI}_3$  perovskite.

highlighted by some of us.<sup>11</sup> The  $\text{MAPbI}_3$  perovskite shows mainly nonoriented structures, either considering materials derived from the one or two steps synthesis.<sup>3,17,21–26</sup>

A possible explanation for the differently oriented structures may lay in the perovskite preparation method, pointing at either the different solvent (GBL vs DMF/DMSO) or the presence of the  $\text{PbCl}_2$  precursor material, or a combination of these two factors. This observation could be related to the improved photovoltaic performance of  $\text{MAPbI}_{3-x}\text{Cl}_x$  and generically to the aforementioned “chlorine effect”, as various works have highlighted the importance of the perovskite morphology for efficient charge separation and solar cell operation.<sup>26,28</sup> Another interesting effect observed in mixed-halide perovskites is the enhanced temporal stability of solar cells based on these materials compared to that of the standard  $\text{MAPbI}_3$ .<sup>12,13</sup>

Here, we investigate the effect of chlorine on the prototypical  $\text{TiO}_2$ /perovskite interface, by state of the art, first-principles electronic structure calculations on extended models. The investigated heterointerface is representative of both conventional dye-sensitized solar cells based on a mesoporous  $\text{TiO}_2$  scaffold and, to some extent, of flat devices in which a compact  $\text{TiO}_2$  film is used as electron selective layer.

We find that the  $\text{MAPbI}_3$  and  $\text{MAPbI}_{3-x}\text{Cl}_x$  perovskites show a higher stability of the (110) surfaces, with  $\text{TiO}_2$  further enhancing the stability of the (110) surface due to the better structural matching between rows of adjacent perovskite surface halides and  $\text{TiO}_2$  undercoordinated titanium atoms. Interfacial chlorine atoms increase the perovskite binding energy to  $\text{TiO}_2$ , possibly contributing to the enhanced temporal stability of the ensuing solar cell devices, as experimentally observed. The interaction of the  $\text{MAPbI}_{3-x}\text{Cl}_x$  perovskite with  $\text{TiO}_2$  modifies the interface electronic structure, leading to a stronger electronic coupling between the titanium d and lead p conduction band states and to a slight  $\text{TiO}_2$  conduction band energy upshift. Most notably, the presence of interfacial chlorine induces an asymmetry in the  $\text{MAPbI}_{3-x}\text{Cl}_x$  perovskite CB edge compared to that of  $\text{MAPbI}_3$ , leading to increased perovskite  $\rightarrow \text{TiO}_2$  charge transfer, which may determine a vectorial charge flow of photogenerated electrons toward the  $\text{TiO}_2$  surface.

Our models are originated from the optimized  $\text{MAPbI}_3$  structure,<sup>15</sup> which was obtained by the experimentally reported

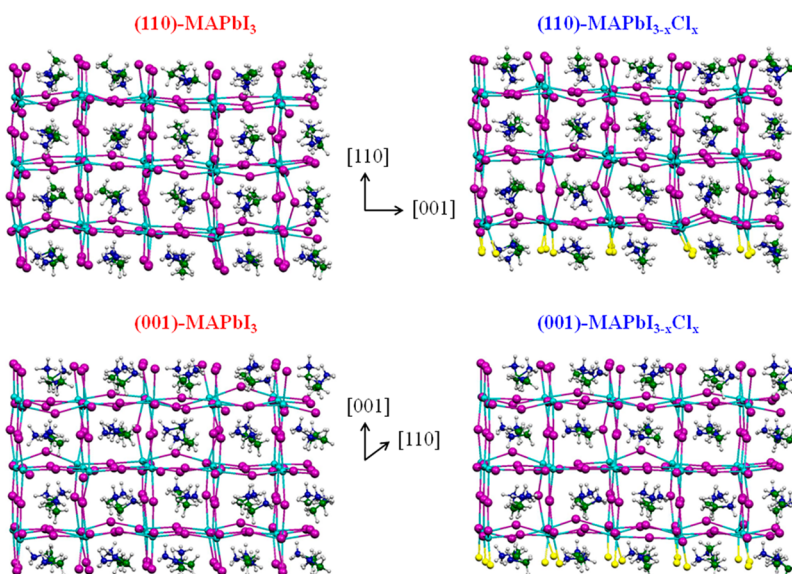


**Figure 1.** Optimized geometrical structures of the (110) and (001) surface slabs for the  $\text{MAPbI}_3$  and  $\text{MAPbI}_{3-x}\text{Cl}_x$  perovskites. Colors: Pb, light blue; I, purple; N, blue; C, green; H, white; Cl, yellow.

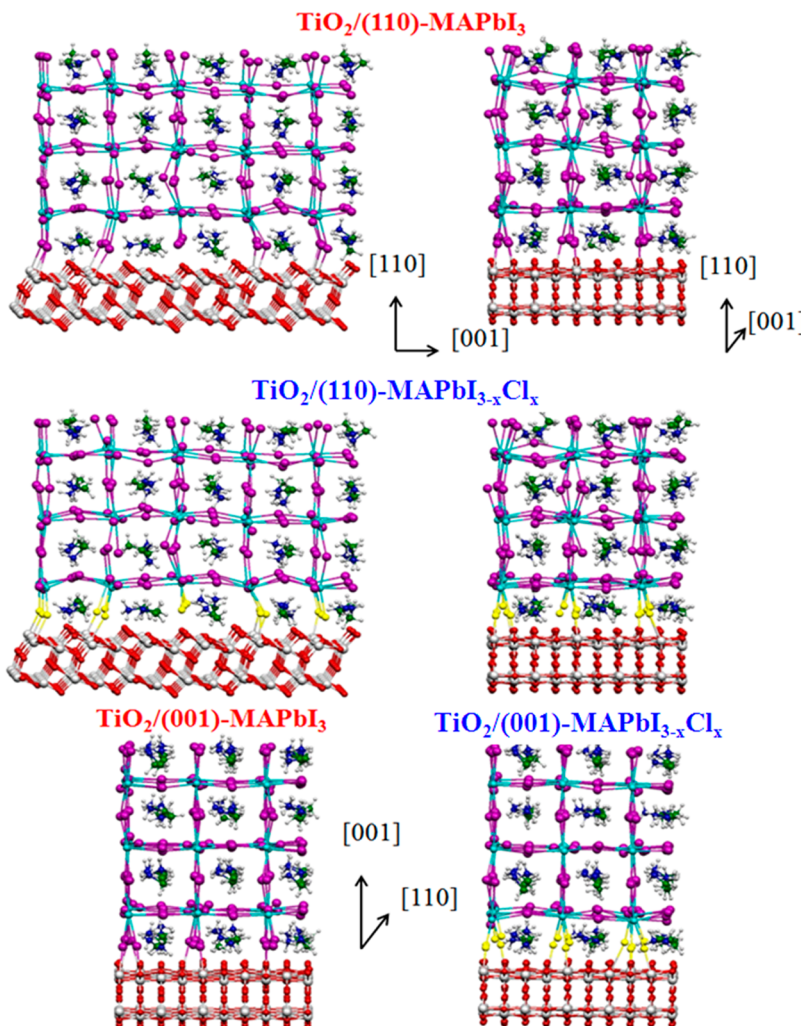


**Figure 2.** Optimized  $\text{TiO}_2$ /perovskite interface structures of the (110) seen along two different orientations and (001) surface slabs for the  $\text{MAPbI}_3$  and  $\text{MAPbI}_{3-x}\text{Cl}_x$  perovskites. Colors: Pb, light blue; I, purple; N, blue; C, green; H, white; Cl, yellow; Ti, gray; O, red.

XRD data by Kawamura et al.,<sup>29</sup> Scheme 1. Our calculated structures, obtained without any symmetry constraints, are conform to the  $I4\text{cm}$  space group proposed by Stoumpos et al.,<sup>30</sup> showing the lack of an inversion symmetry along the crystallographic  $c$  axis. We consider both pseudocubic (001) and tetragonal (110) perovskite surfaces, considering for the isolated slabs the experimental lattice parameters of the tetragonal phase.<sup>27</sup> Thus, although for the (110) surface, we exactly investigate the phase that is stable at room temperature, for the (001) surface, we chose to look at the pseudocubic phase for a better structural matching with the  $\text{TiO}_2$  lattice, see below. We notice, however, that the (001) surfaces of the cubic and tetragonal phases have an identical topology, the (001) surface of the tetragonal phase effectively corresponds to one of the three equivalent surfaces of the cubic phase, so we expect this approximation not to introduce artificial features in our modeling. Although the structural properties of the investigated systems are nicely reproduced by scalar-relativistic (SR) DFT,<sup>15,31</sup> inclusion of spin–orbit coupling (SOC) is crucial for a correct electronic structure description of lead perovskites,<sup>31–33</sup> so SOC is included in the presented electronic structure calculations. We also recently showed that many body perturbation theory including SOC, within the GW approach, can accurately describe the electronic structure and band gap of the investigated hybrid perovskites.<sup>31</sup> The

investigated systems are, however, too large to be subjected to GW calculations, so we retain a SOC-DFT description of the electronic structure of the investigated heterointerfaces, which was shown to qualitatively follow the SOC-GW trends.<sup>31,33</sup>

In line with a recent computational investigation of the  $\text{TiO}_2/\text{MAPbI}_3$  interface,<sup>34</sup> our model system is made by  $3 \times 5 \times 3$  perovskite slabs of  $(\text{CH}_3\text{NH}_3)_{60}\text{Pb}_{45}\text{I}_{150}$  stoichiometry, Figure 1, as from the analysis of perovskites surfaces by Mitzi.<sup>35</sup> Starting from this system, we considered the replacement of 15 iodine surface atoms by chlorine atoms. This choice is justified by the experimental observation that chlorine is basically incorporated into the perovskite lattice only to a very small extent and that it is possibly located at the material surface.<sup>11,18</sup> Because our aim is to study the perovskite interface with  $\text{TiO}_2$ , we use in this case the experimental  $\text{TiO}_2$  cell parameters ( $a = 18.92 \text{ \AA}$ ,  $b = 30.72 \text{ \AA}$ ) to build our supercells, leaving  $10 \text{ \AA}$  vacuum along the nonperiodic direction orthogonal to the surface direction. The resulting (110) optimized  $\text{MAPbI}_3$  slab, Figure 1, has a calculated band gap of  $1.96 \text{ eV}$ , by SR-DFT, which reduces to  $1.32 \text{ eV}$  upon inclusion of SOC.<sup>31,32</sup> The chosen setup introduces a lattice mismatch for the (110) surfaces of only  $+0.36$  and  $+1.92\%$  along the  $\text{TiO}_2$   $a$  and  $b$  directions, and of  $+0.75$  and  $-1.85\%$ , respectively, for the pseudocubic (001) surfaces. Notably, for the tetragonal (001)

surface a lattice mismatch of  $-6.40$  and  $-13.52\%$  is found with the same  $\text{TiO}_2$  slab, which would introduce excessive strain into the perovskite subsystem. For comparison, when using the experimental cell parameters for the (110)  $\text{MAPbI}_3$  surface, the band gap only slightly varies ( $1.87$  eV), with a corresponding  $0.4$  eV total energy decrease, suggesting that a minimal strain is introduced by the small lattice mismatch between the two materials. The calculated band gap values are higher than those found for the bulk tetragonal phase of the  $\text{CH}_3\text{NH}_3\text{PbI}_3$  perovskite at the same level of theory,  $1.66$  and  $0.60$  eV by SR- and SOC-DFT, respectively,<sup>31</sup> as expected when moving from a periodic to a confined system. Notably, by doubling the perovskite slab along the nonperiodic [110] direction, we find for the (110) surface slab a band gap value by SR-DFT of  $1.55$  eV, comparable to that of calculated for the bulk at the same level of theory. The investigated  $\text{MAPbI}_3$  (001) surface slab has larger band-gaps,  $2.37$  and  $1.50$  eV by SR- and SOC-DFT respectively. Replacement of surface iodine by chlorine atoms basically does not affect the band gap because chlorine introduces occupied levels below the valence band edge;<sup>15</sup> see below.

The perovskite models were “deposited” onto a  $5 \times 3 \times 2$  slab of anatase  $\text{TiO}_2$  made by  $120$   $\text{TiO}_2$  units, exposing the majority (011) surface; see Figure 2.

Given the slab surface stoichiometry, the  $\text{TiO}_2$ /perovskite interaction occurs mainly through the binding of perovskite halide atoms to under-coordinated Ti(IV) atoms of the  $\text{TiO}_2$  surface.<sup>34</sup> Notably, the isolated (110) slab is slightly more stable than the corresponding (001) slab, with a total energy difference of  $0.7$  and  $0.1$  eV for the  $\text{MAPbI}_3$  and  $\text{MAPbI}_{3-x}\text{Cl}_x$  perovskites, see Table 1. Notice that these surface energies are likely to be

**Table 1. Calculated Relative Energies<sup>a</sup> between the (110) and (001) Surfaces for the Isolated and  $\text{TiO}_2$ -Adsorbed Slabs of  $\text{MAPbI}_3$  and  $\text{MAPbI}_{3-x}\text{Cl}_x$ <sup>b</sup>**

	(110)			(001)		
	slab		slab@ $\text{TiO}_2$	slab		slab@ $\text{TiO}_2$
	rel. en.	rel. en.	bind. en.	rel. en.	rel. en.	bind. en.
$\text{MAPbI}_3$	0.0	0.0	-24.2	0.7	7.0	-17.8
$\text{MAPbI}_{3-x}\text{Cl}_x$	0.0	0.0	-27.3	0.1	6.5	-20.9

<sup>a</sup>Denoted “rel. en.”, in eV. <sup>b</sup>For the slabs@ $\text{TiO}_2$ , we also reported the calculated binding energies, denoted “bind. en.”, in eV.

affected by the different phase (tetragonal vs pseudocubic) simulated here and by the employment of  $\text{TiO}_2$  cell parameters, so this data must be taken with care.

Upon adsorption of the investigated perovskites onto the  $\text{TiO}_2$  surface, the calculated energetics change substantially, with the (110) surface now favored by  $7.0$  and  $6.5$  eV (total energy difference) against the (001) surface, for  $\text{MAPbI}_3$  and  $\text{MAPbI}_{3-x}\text{Cl}_x$  perovskites, respectively, that is, by ca.  $0.45$  eV per interacting surface halide. Notably, this data is exempt from the issues concerning the different phase stability discussed above because here we are looking at a difference (between the (110) and (001) surfaces) of energy differences (between to  $\text{MAPbI}_3$  and  $\text{MAPbI}_{3-x}\text{Cl}_x$ ). Consistently, the (110) surfaces are calculated to show a higher (ca.  $7$  eV) binding energy to  $\text{TiO}_2$  surface compared to that of the (001) surfaces. Even more important, for both the (110) and (001) adsorbed surfaces, the presence of interfacial chlorine atoms is calculated to induce an

increased perovskite binding energy to the  $\text{TiO}_2$  surface, calculated as the difference between the interacting  $\text{TiO}_2$ /perovskite and the isolated fragments, of ca.  $3$  eV in terms of total energy difference or ca.  $0.2$  eV per interacting surface halide, compared to that of  $\text{MAPbI}_3$ . This data could possibly be related to the observed enhanced temporal stability of devices incorporating mixed halide perovskites, and it points at the perovskite adhesion to the  $\text{TiO}_2$  substrate as a possible cause, among other factors, of solar cell deterioration.

To summarize, the (110) surfaces are strongly stabilized by interaction with  $\text{TiO}_2$ , with interfacial chlorine atoms leading to additionally higher binding energy to  $\text{TiO}_2$  in  $\text{MAPbI}_{3-x}\text{Cl}_x$  compared to that of  $\text{MAPbI}_3$ .

To understand the reason underlying the preferential (110) surface interaction with  $\text{TiO}_2$ , we investigated the radial distribution function of the X-Ti (X = I or Cl) bond distances calculated for the  $\text{MAPbI}_3$  and  $\text{MAPbI}_{3-x}\text{Cl}_x$  perovskites interacting with  $\text{TiO}_2$  via the (110) or (001) surfaces. For both perovskites, adsorption through the (110) surface leads to an enhanced number of shorter X-I bonds compared to the same material adsorbed through the (001) surface, see Supporting Information. This structural analysis is clearly consistent with the calculated stabilization of the (110) surface interaction with  $\text{TiO}_2$  compared to the (001) surfaces, and it appears to be originated by the better structural matching of the former compared to the latter surface. This is, in turn, originated by the sizable tilting (ca.  $22^\circ$ ) of the  $\text{PbX}_6$  octahedra around the  $c$  axis (of  $a^0b^0c^-$  in the Glazer notation),<sup>33</sup> introducing alternatively tilted (110) planes along the [001] direction (see Figures 1 and 2) as opposed to the almost perfectly stacked (001) planes. This analysis also shows that shorter X-Ti bonds are formed in both the (110) and (001) cases by the interfacial chlorine atoms compared to iodine, as expected on the basis of the smaller chlorine size and stronger propensity to form ionic bonds with undercoordinated surface Ti(IV) atoms; see Supporting Information.

The calculated interface electronic structure, is analyzed in terms of aligned (to the Pb 5d peaks) partial Density of States (PDOS) in the conduction band region in Figure 3. We need to stress here that, as previously reported,<sup>34</sup> we do not expect in principle our SOC-DFT calculations to quantitatively reproduce the  $\text{TiO}_2$ /perovskite alignment of energy levels compared to experimental data due to possible shortcomings in the description of both  $\text{TiO}_2$  and organohalide perovskites by GGA-DFT. Nevertheless, the comparative effect of interfacial chlorine vs iodine on the interacting energy levels of  $\text{TiO}_2$ /  $\text{MAPbI}_3$  and  $\text{TiO}_2$ /  $\text{MAPbI}_{3-x}\text{Cl}_x$  is expected to be accurately reproduced even if the absolute energy alignment could be relatively inaccurate.

As previously reported, chlorine atoms contribute occupied states  $\sim 1$  eV below and above the valence and conduction band edges, respectively;<sup>15</sup> their effect on the low-energy unoccupied PDOS is, thus, mainly indirect. The perovskite CB edge, summing the contribution from Pb and X atoms, is calculated to lay ca.  $0.8$  eV above the  $\text{TiO}_2$  CB edge, Figure 3. This value is overestimated compared to experimental band edge offsets of  $0.4$  eV by Lindblad et al., obtained directly measuring the occupied energy levels of the  $\text{MAPbI}_3$  perovskite as well as the underneath  $\text{TiO}_2$ ,<sup>36</sup> which should, thus, closely resemble the situation simulated here. Apart from the aforementioned inherent limitations of GGA-DFT (albeit including SOC), such an overestimate is due to the confinement imposed by the considered slabs (both  $\text{TiO}_2$  and perovskite) of limited thickness. By extrapolating the SR-DFT results obtained for the larger (110)

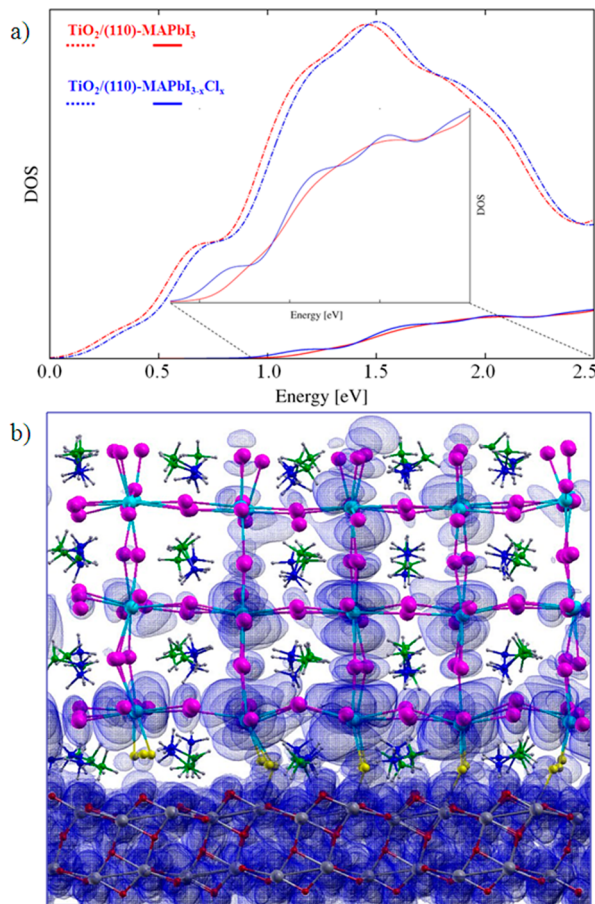


**Figure 3.** (a) Partial density of states (DOS) with summed contributions from  $\text{TiO}_2$  (dashed) and perovskite (solid) contributions for the (110)  $\text{TiO}_2/\text{MAPbI}_3$  (red) and  $\text{TiO}_2/\text{MAPbI}_{3-x}\text{Cl}_x$  (blue) interfaces. The zero of the energy is set at the  $\text{TiO}_2$  conduction band minimum. (b) Isodensity plot a typical  $\text{TiO}_2/\text{MAPbI}_{3-x}\text{Cl}_x$  unoccupied state lying at ca. 1.3 eV above the CB edge.

perovskite slab, showing a comparable band gap compared to the bulk, we estimate the error on the band gap due to the slab thickness to amount to ca. 0.3 eV, to be distributed between the occupied and unoccupied states. Thus, overall, the relative alignment of unoccupied  $\text{TiO}_2$ /perovskite energy levels is reproduced (to the level of  $\pm 0.2$  eV) by GGA-DFT, including SOC against experimental data. Once again, this level of accuracy is referred to the absolute energy alignment compared to experimental data, whereas the relative effect of chlorine on the interface is expected to be accurately reproduced by SOC-DFT.

Despite the indirect effect on the unoccupied PDOS, the  $\text{MAPbI}_{3-x}\text{Cl}_x$  perovskite CB edge is sizably perturbed by the presence of chlorine atoms compared to  $\text{MAPbI}_3$ , inset of Figure 3. This is likely to be due to the stronger interaction of the perovskite with  $\text{TiO}_2$ , leading to enhanced interfacial coupling between the unoccupied titanium d orbitals and lead p orbitals, constituting the  $\text{TiO}_2$ /perovskite conduction bands, respectively; see a characteristic unoccupied state for the  $\text{TiO}_2/\text{MAPbI}_{3-x}\text{Cl}_x$  system in Figure 3b showing a polarization of the perovskite states toward the  $\text{TiO}_2$  surface.

To quantify the extent of charge transfer across the  $\text{TiO}_2$ /perovskite interface, we have resorted to a charge displacement (CD) analysis,<sup>37,38</sup> which allows us to visualize the displacement of charge occurring from the non interacting  $\text{TiO}_2$  and perovskites fragments to the interacting heterointerface, see ref 37 for further details. The resulting CD curves for (110)  $\text{TiO}_2/\text{MAPbI}_3$  and  $\text{TiO}_2/\text{MAPbI}_{3-x}\text{Cl}_x$  interfaces are reported in Figure 4 and shows a slight increase in charge donation to  $\text{TiO}_2$  in the case of the  $\text{MAPbI}_{3-x}\text{Cl}_x$  perovskite, along with a strong polarization in both cases, signaled by the strong CD variation across the interface region. This leads to an increased charge accumulation at the interface for the  $\text{MAPbI}_{3-x}\text{Cl}_x$  compared to the  $\text{MAPbI}_3$  perovskite, which we quantified in 0.85 vs. 0.61 electrons, respectively.

As a consequence of the stronger  $\text{TiO}_2$ /perovskite interaction, the  $\text{TiO}_2$  CB is shifted at higher energy (by ca. 0.05–0.10 eV) in the  $\text{TiO}_2/\text{MAPbI}_{3-x}\text{Cl}_x$  system interface compared to  $\text{TiO}_2/\text{MAPbI}_3$ , Figure 3, a typical effect observed

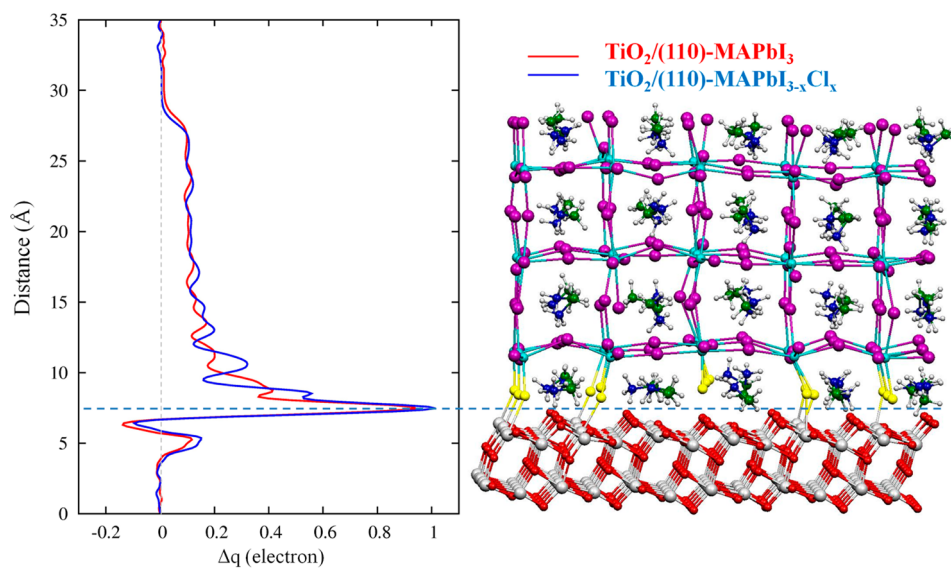


**Figure 4.** Charge displacement analysis of the  $\text{TiO}_2$ /perovskite interface for the (110)  $\text{TiO}_2/\text{MAPbI}_3$  (red) and  $\text{TiO}_2/\text{MAPbI}_{3-x}\text{Cl}_x$  (blue) systems. The strong polarization at the interface between the perovskite and the  $\text{TiO}_2$  surfaces is evidenced by the change of sign of the displaced charge ( $\Delta q$ , electrons) at the interface (dashed horizontal line).

also in  $\text{TiO}_2$  sensitized by molecular dyes of increasing charge donation capability.<sup>37</sup> This is also manifested as a perturbation to the electrostatic potential of the interacting  $\text{TiO}_2/\text{MAPbI}_{3-x}\text{Cl}_x$  system in the vacuum region; see Supporting Information. The observed CB shift could contribute to higher open circuit voltages in perovskite solar cells employing a mesoporous  $\text{TiO}_2$ . The  $\text{TiO}_2$  CB upshift, which in dye-sensitized solar cells could cause a reduction of the photocurrent due to a decrease of the driving force for electron injection, is possibly compensated here by a stronger interfacial coupling.

In summary, we have investigated, by first-principles computational methods on realistic models, the effect of surface chlorine atoms on the morphology and electronic structure of perovskite thin films at the interface with  $\text{TiO}_2$ . Although perovskite solar cells can function with or without a mesoporous  $\text{TiO}_2$  layer, a compact  $\text{TiO}_2$  layer is incorporated in most devices to act as an electron-selective layer; thus, the  $\text{TiO}_2/\text{perovskite}$  interface is of paramount importance for both type of devices. We considered, in particular, the competition between formation of the supposedly more abundant (110) and (001) perovskite surfaces on anatase  $\text{TiO}_2$ . Our main findings are the following:

- (1) The  $\text{MAPbI}_3$  and  $\text{MAPbI}_{3-x}\text{Cl}_x$  perovskites tend to preferentially grow (110) surfaces on  $\text{TiO}_2$ . Thus,  $\text{TiO}_2$  strongly amplifies the slightly higher stability of the (110) surfaces compared to (001) in the isolated slabs.
- (2) The (110)-oriented preferential growth is due to the better structural matching between rows of adjacent perovskite surface halides and  $\text{TiO}_2$  undercoordinated titanium atoms due to octahedral tilting in the perovskite tetragonal structures typical of  $\text{MAPbI}_3$  and  $\text{MAPbI}_{3-x}\text{Cl}_x$ .
- (3) Interfacial chlorine atoms increase the binding energy of the (110) surface to  $\text{TiO}_2$  in  $\text{MAPbI}_{3-x}\text{Cl}_x$  compared to  $\text{MAPbI}_3$ . The higher calculated binding energy of the  $\text{MAPbI}_{3-x}\text{Cl}_x$  perovskite on  $\text{TiO}_2$  compared to  $\text{MAPbI}_3$  could contribute to enhance the temporal stability of the ensuing solar cell devices.
- (4) The interaction of the  $\text{MAPbI}_{3-x}\text{Cl}_x$  perovskite with  $\text{TiO}_2$  modifies the interface electronic structure, leading to a stronger interfacial coupling between the titanium d and lead p conduction band states, favoring higher electron injection, and to a slight  $\text{TiO}_2$  conduction band energy upshift.

We believe our study to rationalize a number of experimental observables, casting a direct connection between the perovskite preparation method/employed solvent or composition and the morphology and electronic properties of the resulting perovskite films. In terms of connection to solar cell operation, our findings could contribute to explain the reduced carrier recombination observed in  $\text{MAPbI}_{3-x}\text{Cl}_x$  and, in general, in mixed halide perovskites compared to  $\text{MAPbI}_3$ . The stronger interfacial coupling mediated by chlorine atoms could contribute to higher electron collection (due to the improved electron transfer to  $\text{TiO}_2$ ) and slightly improved open circuit voltage in mesoporous  $\text{TiO}_2$ -based devices due to the a possible  $\text{TiO}_2$  conduction band upshift.

The results of our first-principles modeling, fully consistent with available experimental data, may constitute the basis for a further exploitation of perovskite solar cells and may stimulate further experimental studies to reveal the elusive presence of chlorine in mixed halide perovskites.

## EXPERIMENTAL METHODS

Geometry optimizations have been carried out at PBE-GGA<sup>39</sup> level with SIESTA 3.0 program package<sup>40</sup> using a DZ basis set along with nonrelativistic pseudopotentials for Ti, O, C, N, and H atoms. Pb atoms are treated with the WC-GGA<sup>41</sup> relativistic pseudopotential. Electrons from O, N, and C 2s and 2p; H 1s; Ti 4s and 3d; and Pb 6s, 6p, and 5d shells explicitly included in the calculations. Spin orbit interactions are not included in SIESTA calculations. A value of 100 Ry is used as plane-wave cutoff for the grid. Electronic structure analyses were performed at the same PBE-GGA<sup>39</sup> level used for geometry optimizations, with the Quantum-Espresso program package<sup>42</sup> on the structures optimized by SIESTA. Electron–ion interactions were described by ultrasoft pseudopotentials with electrons from S 3s and 3p; O, N, and C 2s and 2p; H 1s; Ti 3s, 3p, 3d, and 4s; and Pb 6s, 6p, and 5d shells explicitly included in the calculations. Plane-wave basis set cutoffs for the smooth part of the wave functions and the augmented density were 25 and 200 Ry, respectively. Electronic structure calculations were performed at the scalar relativistic level and included spin–orbit coupling. We previously checked that SIESTA and Quantum Espresso provide perfectly coherent results for the  $\text{MAPbI}_3$  perovskite slab and for its interface with  $\text{TiO}_2$ .<sup>34</sup> We are, thus, confident on the conformity of the two codes, and here, we exploit the efficiency of SIESTA for geometry optimizations and the SOC-DFT implementation of Quantum Espresso.<sup>43</sup>

## ASSOCIATED CONTENT

### Supporting Information

Radial distribution functions and plots of the electrostatic potential. This material is available free of charge via the Internet at <http://pubs.acs.org/>.

## AUTHOR INFORMATION

### Corresponding Authors

\*E. Mosconi. E-mail: edoardo@thch.unipg.it.

\*F. De Angelis. E-mail: filippo@thch.unipg.it.

### Notes

The authors declare no competing financial interest.

## ACKNOWLEDGMENTS

The research leading to these results has received funding from the European Union Seventh Framework Programme [FP7/2007-2013] under grant agreement no. 604032 of the MESO project.

## REFERENCES

- (1) Kojima, A.; Teshima, K.; Shirai, Y.; Miyasaka, T. Organometal Halide Perovskites as Visible-Light Sensitizers for Photovoltaic Cells. *J. Am. Chem. Soc.* **2009**, *131*, 6050–6051.
- (2) Liu, M.; Johnston, M. B.; Snaith, H. J. Efficient planar heterojunction perovskite solar cells by vapour deposition. *Nature* **2013**, *501*, 395–398.
- (3) Burschka, J.; Pellet, N.; Moon, S.-J.; Humphry-Baker, R.; Gao, P.; Nazeeruddin, M. K.; Grätzel, M. Sequential Deposition As a Route to High-Performance Perovskite-Sensitized Solar Cells. *Nature* **2013**, *499*, 316–319.
- (4) Ball, J. M.; Lee, M. M.; Hey, A.; Snaith, H. J. Low-Temperature Processed Meso-Superstructured to Thin-Film Perovskite Solar Cells. *Energy Environ. Sci.* **2013**, *6*, 1739–1743.
- (5) Docampo, P.; Ball, J. M.; Darwich, M.; Eperon, G. E.; Snaith, H. J. Efficient Organometal Trihalide Perovskite Planar-Heterojunction Solar Cells on Flexible Polymer Substrates. *Nat. Commun.* **2013**, *4*.

- (6) Malinkiewicz, O.; Yella, A.; Lee, Y. H.; Espallargas, G. M.; Graetzel, M.; Nazeeruddin, M. K.; Bolink, H. J. Perovskite Solar Cells Employing Organic Charge-Transport Layers. *Nat. Photonics* **2014**, *8*, 128–132.
- (7) Etgar, L.; Gao, P.; Xue, Z.; Peng, Q.; Chandiran, A. K.; Liu, B.; Nazeeruddin, M. K.; Grätzel, M. Mesoscopic  $\text{CH}_3\text{NH}_3\text{PbI}_3/\text{TiO}_2$  Heterojunction Solar Cells. *J. Am. Chem. Soc.* **2012**, *134*, 17396–17399.
- (8) Lee, M. M.; Teuscher, J.; Miyasaka, T.; Murakami, T. N.; Snaith, H. J. Efficient Hybrid Solar Cells Based on Meso-Superstructured Organometal Halide Perovskites. *Science* **2012**, *338*, 643–647.
- (9) Stranks, S. D.; Eperon, G. E.; Grancini, G.; Menelaou, C.; Alcocer, M. J. P.; Leijtens, T.; Herz, L. M.; Petrozza, A.; Snaith, H. J. Electron-Hole Diffusion Lengths Exceeding 1 Micrometer in an Organometal Trihalide Perovskite Absorber. *Science* **2013**, *342*, 341–344.
- (10) Wehrenfennig, C.; Eperon, G. E.; Johnston, M. B.; Snaith, H. J.; Herz, L. M. High Charge Carrier Mobilities and Lifetimes in Organolead Trihalide Perovskites. *Adv. Mater.* **2014**, *26*, 1584–1589.
- (11) Colella, S.; Mosconi, E.; Fedeli, P.; Listorti, A.; Gazza, F.; Orlandi, F.; Ferro, P.; Besagni, T.; Rizzo, A.; Calestani, G.; et al. MAPbI<sub>3</sub>-xCl<sub>x</sub> Mixed Halide Perovskite for Hybrid Solar Cells: The Role of Chloride as Dopant on the Transport and Structural Properties. *Chem. Mater.* **2013**, *25*, 4613–4618.
- (12) Noh, J. H.; Im, S. H.; Heo, J. H.; Mandal, T. N.; Seok, S. I. Chemical Management for Colorful, Efficient, and Stable Inorganic–Organic Hybrid Nanostructured Solar Cells. *Nano Lett.* **2013**, *13*, 1764–1769.
- (13) Suarez, B.; Gonzalez-Pedro, V.; Ripolles, T. S.; Sanchez, R. S.; Otero, L.; Mora-Sero, I. Recombination Study of Combined Halides (Cl, Br, I) Perovskite Solar Cells. *J. Phys. Chem. Lett.* **2014**, *1628–1635*.
- (14) Gonzalez-Pedro, V.; Juarez-Perez, E. J.; Arsyad, W.-S.; Barea, E. M.; Fabregat-Santiago, F.; Mora-Sero, I.; Bisquert, J. General Working Principles of  $\text{CH}_3\text{NH}_3\text{PbX}_3$  Perovskite Solar Cells. *Nano Lett.* **2014**, *14*, 888–893.
- (15) Mosconi, E.; Amat, A.; Nazeeruddin, M. K.; Grätzel, M.; De Angelis, F. First-Principles Modeling of Mixed Halide Organometal Perovskites for Photovoltaic Applications. *J. Phys. Chem. C* **2013**, *117*, 13902–13913.
- (16) Yamada, K.; Nakada, K.; Takeuchi, Y.; Nawa, K.; Yamane, Y. Tunable Perovskite Semiconductor  $\text{CH}_3\text{NH}_3\text{SnX}_3$  (X: Cl, Br, or I) Characterized by X-ray and DTA. *Bull. Chem. Soc. Jpn.* **2011**, *84*, 926–932.
- (17) Zhao, Y.; Zhu, K. CH<sub>3</sub>NH<sub>3</sub>Cl-Assisted One-Step Solution Growth of CH<sub>3</sub>NH<sub>3</sub>PbI<sub>3</sub>: Structure, Charge-Carrier Dynamics, and Photovoltaic Properties of Perovskite Solar Cells. *J. Phys. Chem. C* **2014**, *118*, 9412–9418.
- (18) Edri, E.; Kirmayer, S.; Kulkarni, M.; Hodes, G.; Cahen, D. Chloride Inclusion and Hole Transport Material Doping to Improve Methyl Ammonium Lead Bromide Perovskite-Based High Open-Circuit Voltage Solar Cells. *J. Phys. Chem. Lett.* **2014**, *5*, 429–433.
- (19) D’Innocenzo, V.; Grancini, G.; Alcocer, M. J. P.; Kandada, A. R. S.; Stranks, S. D.; Lee, M. M.; Lanzani, G.; Snaith, H. J.; Petrozza, A. Excitons versus Free Charges in Organo-Lead Tri-Halide Perovskites. *Nat. Commun.* **2014**, *5*, 3586.
- (20) Conings, B.; Baeten, L.; De Dobbelaere, C.; D’Haen, J.; Manca, J.; Boyen, H.-G. Perovskite-Based Hybrid Solar Cells Exceeding 10% Efficiency with High Reproducibility Using a Thin Film Sandwich Approach. *Adv. Mater.* **2013**, *n/a–n/a*.
- (21) Baikie, T.; Fang, Y.; Kadro, J. M.; Schreyer, M.; Wei, F.; Mhaisalkar, S. G.; Grätzel, M.; White, T. J. Synthesis and Crystal Chemistry of the Hybrid Perovskite (CH<sub>3</sub>NH<sub>3</sub>)PbI<sub>3</sub> for Solid-State Sensitized Solar Cell Applications. *J. Mater. Chem. A* **2013**, *1*, 5628–5641.
- (22) Heo, J. H.; Im, S. H.; Noh, J. H.; Mandal, T. N.; Lim, C.-S.; Chang, J. A.; Lee, Y. H.; Kim, H.-j.; Sarkar, A.; Nazeeruddin Md, K.; et al. Efficient Inorganic–Organic Hybrid Heterojunction Solar Cells Containing Perovskite Compound and Polymeric Hole Conductors. *Nat. Photonics* **2013**, *7*, 486–491.
- (23) Kim, H.-B.; Choi, H.; Jeong, J.; Kim, S.; Walker, B.; Song, S.; Kim, J. Y. Mixed Solvents for the Optimization of Morphology in Solution-Processed, Inverted-Type Perovskite/Fullerene Hybrid Solar Cells. *Nanoscale* **2014**, *6*, 6679–6683.
- (24) Chen, Q.; Zhou, H.; Hong, Z.; Luo, S.; Duan, H.-S.; Wang, H.-H.; Liu, Y.; Li, G.; Yang, Y. Planar Heterojunction Perovskite Solar Cells via Vapor-Assisted Solution Process. *J. Am. Chem. Soc.* **2013**, *136*, 622–625.
- (25) Qiu, J.; Qiu, Y.; Yan, K.; Zhong, M.; Mu, C.; Yan, H.; Yang, S. All-Solid-State Hybrid Solar Cells Based on a New Organometal Halide Perovskite Sensitizer and One-Dimensional TiO<sub>2</sub> Nanowire Arrays. *Nanoscale* **2013**, *5*, 3245–3248.
- (26) Liang, P.-W.; Liao, C.-Y.; Chueh, C.-C.; Zuo, F.; Williams, S. T.; Xin, X.-K.; Lin, J.; Jen, A. K. Y. Additive Enhanced Crystallization of Solution-Processed Perovskite for Highly Efficient Planar-Heterojunction Solar Cells. *Adv. Mater.* **2014**, DOI: 10.1002/adma.201400231.
- (27) Poglitsch, A.; Weber, D. Dynamic Disorder in Methylammoniumtrihalogenoplumbates (II) Observed by Millimeter-Wave Spectroscopy. *J. Chem. Phys.* **1987**, *87*, 6373–6378.
- (28) Eperon, G. E.; Burlakov, V. M.; Docampo, P.; Goriely, A.; Snaith, H. J. Morphological Control for High Performance, Solution-Processed Planar Heterojunction Perovskite Solar Cells. *Adv. Funct. Mater.* **2014**, *24*, 151–157.
- (29) Kawamura, Y.; Mashiyama, H.; Hasebe, K. Structural Study on Cubic-Tetragonal Transition of CH<sub>3</sub>NH<sub>3</sub>PbI<sub>3</sub>. *J. Phys. Soc. Jpn.* **2002**, *71*, 1694.
- (30) Stoumpos, C. C.; Malliakas, C. D.; Kanatzidis, M. G. Semiconducting Tin and Lead Iodide Perovskites with Organic Cations: Phase Transitions, High Mobilities, and Near-Infrared Photoluminescent Properties. *Inorg. Chem.* **2013**, *52*, 9019–9038.
- (31) Umari, P.; Mosconi, E.; De Angelis, F. Relativistic GW Calculations on CH<sub>3</sub>NH<sub>3</sub>PbI<sub>3</sub> and CH<sub>3</sub>NH<sub>3</sub>SnI<sub>3</sub> Perovskites for Solar Cell Applications. *Sci. Rep.* **2014**, *4*, 4467.
- (32) Even, J.; Pedesseau, L.; Jancu, J.-M.; Katan, C. Importance of Spin–Orbit Coupling in Hybrid Organic/Inorganic Perovskites for Photovoltaic Applications. *J. Phys. Chem. Lett.* **2013**, *4*, 2999–3005.
- (33) Amat, A.; Mosconi, E.; Ronca, E.; Quart, C.; Umari, P.; Nazeeruddin, M. K.; Grätzel, M.; De Angelis, F. Cation-Induced Band-Gap Tuning in Organohalide Perovskites: Interplay of Spin–Orbit Coupling and Octahedra Tilting. *Nano Lett.* **2014**, *14*, 3608–3616.
- (34) Roati, V.; Mosconi, E.; Listorti, A.; Colella, S.; Gigli, G.; De Angelis, F. Stark Effect in Perovskite/TiO<sub>2</sub> Solar Cells: Evidence of Local Interfacial Order. *Nano Lett.* **2014**, *14*, 2168–2174.
- (35) Mitzi, D. B. Solution-Processed Inorganic Semiconductors. *J. Mater. Chem.* **2004**, *14*, 2355–2365.
- (36) Lindblad, R.; Bi, D.; Park, B.-w.; Oscarsson, J.; Gorgoi, M.; Siegbahn, H.; Odellius, M.; Johansson, E. M. J.; Rensmo, H. Electronic Structure of TiO<sub>2</sub>/CH<sub>3</sub>NH<sub>3</sub>PbI<sub>3</sub> Perovskite Solar Cell Interfaces. *J. Phys. Chem. Lett.* **2014**, *5*, 648–653.
- (37) Ronca, E.; Pastore, M.; Belpassi, L.; Tarantelli, F.; De Angelis, F. Influence of the Dye Molecular Structure on The TiO<sub>2</sub> Conduction Band in Dye-Sensitized Solar Cells: Disentangling Charge Transfer and Electrostatic Effects. *Energy Environ. Sci.* **2013**, *6*, 183–193.
- (38) Belpassi, L.; Infante, I.; Tarantelli, F.; Visscher, L. The Chemical Bond between Au(I) and the Noble Gases. Comparative Study of NgAuF and NgAu<sup>+</sup> (Ng = Ar, Kr, Xe) by Density Functional and Coupled Cluster Methods. *J. Am. Chem. Soc.* **2008**, *130*, 1048–1060.
- (39) Perdew, J. P.; Burke, K.; Ernzerhof, M. Generalized Gradient Approximation Made Simple. *Phys. Rev. Lett.* **1996**, *77*, 3865–3868.
- (40) José, M. S.; Emilio, A.; Julian, D. G.; Alberto, G.; Javier, J.; Pablo, O.; Daniel, S.-P. The SIESTA Method for Ab Initio Order–N Materials Simulation. *J. Phys.: Condens. Matter* **2002**, *14*, 2745.
- (41) Wu, Z.; Cohen, R. E. More Accurate Generalized Gradient Approximation for Solids. *Phys. Rev. B* **2006**, *73*, 235116.
- (42) Giannozzi, P.; Baroni, S.; Bonini, N.; Calandra, M.; Car, R.; Cavazzoni, C.; Ceresoli, D.; Guido, L. C.; Cococcioni, M.; Dabo, I.; et al. QUANTUM ESPRESSO: A Modular and Open-Source Software Project for Quantum Simulations of Materials. *J. Phys.: Condens. Matter* **2009**, *21*, 395502.
- (43) Dal Corso, A.; Conte Mosca, A. Spin–Orbit Coupling with Ultrasoft Pseudopotentials: Application to Au and Pt. *Phys. Rev. B* **2005**, *71*, 115106.